Journal of Computational Physics **160,** 623–648 (2000)
doi:10.1006/jcph.2000.6478, available online at http://www.idealibrary.com on IDEAL®

Mass Flux Schemes and Connection to Shock Instability

Meng-Sing Liou

Turbomachinery and Propulsion Systems Division, NASA Glenn Research Center at Lewis Field, Cleveland, Ohio 44135

Received November 24, 1998; revised February 10, 2000

We analyze numerical mass fluxes with an emphasis on their capability for accurately capturing shock and contact discontinuities. The study of mass flux is useful because it is the term common to all conservation equations and the numerical diffusivity introduced in it bears a direct consequence to the prediction of contact (stationary and moving) discontinuities, which are considered to be the limiting case of the boundary layer. We examine several prominent numerical flux schemes and analyze the structure of numerical diffusivity. This leads to a detailed investigation into the cause of certain catastrophic breakdowns by some numerical flux schemes. In particular, we identify the dissipative terms that are responsible for shock instabilities, such as the odd–even decoupling and the so-called "carbuncle phenomenon." As a result, we propose a conjecture stating the connection of the pressure difference term to these multidimensional shock instabilities and hence a cure to those difficulties. The validity of this conjecture has been confirmed by examining a wide class of upwind schemes. The conjecture is useful to the flux function development, for it indicates whether the flux scheme under consideration will be afflicted with these kinds of failings. Thus, a class of shock-stable schemes can be identified. Interestingly, a shock-stable scheme's self-correcting capability is demonstrated with respect to carbuncle-contaminated profiles for flows at both low supersonic and high Mach numbers.

Key Words: upwind methods; mass flux; shock (carbuncle) instability; AUSM schemes.

1. INTRODUCTION

Numerical representation of inviscid fluxes, namely the numerical flux function, has been a subject of intensive effort by many researchers during the past three decades. We claim in this paper that it plays a central role in affecting the success of a calculation, especially with regard to robustness and accuracy. Despite the enormous progress achieved, deficiencies

0021-9991/00

have also been experienced. The framework of the Riemann solution by Godunov [1] has dominated the upwind community and has been hailed as the approach to follow or the standard for benchmarking any new schemes. This is rightly so for a large class of problems. Yet less well known are the fundamental deficiencies of the Godunov scheme and its approximation schemes. The so-called shock instability in multidimensions [2] is a prime example of this fundamental failure, along with the nonexistence of a solution for the strong receding (or double rarefaction) flows [3]. These two failures are believed to be caused by different mechanisms. We will address the first issue in this paper.

We show in this paper that the mass flux is the most essential element in constructing a robust and accurate numerical flux that is free of the above two anomalies. This may be understood by realizing that the mass flux is common to the convective part in every conservation equation of the fluid flows. It also provides a means for coupling all equations. We demonstrate a set of simple and effective tools/criteria for designing the mass flux, which in turn delivers robustness and accuracy for all the stringent test problems known to the author, some of which are failed by the Godunov scheme and other prominent schemes such as those by Roe [4] and Osher and Solomon [5]. As a result of this investigation, we have identified that the root of the multidimensional shock instability, which is manifested by the odd–even decoupling and "carbuncle" phenomena, is the existence of a pressure term in the mass flux. Hence, identification of the pressure term in the mass flux of a scheme can provide a quick check as to its predictability for these problems. This claim is further supported in the numerical tests because the anomalies will disappear with the removal of this pressure term in the original schemes.

To demonstrate the properties analyzed, we will consider mostly the unsteady calculations because they generally shed more light on the capability of the scheme in terms of robustness and accuracy.

The paper is organized as follows. In Section 2, we give an interesting form of inviscid flux in generalized 3D coordinates. Then we present in Section 3 a general formulation of numerical flux, especially the mass flux. The shock instability is analyzed in detail in Section 4. We conclude this paper with summary remarks.

2. INVISCID FLUX

For the purposes of this paper, it is only necessary to consider the Euler equations, which we write specifically for fluids obeying the ideal gas law in multi-space dimensions,

$$\frac{\partial \mathbf{U}}{\partial t} + \operatorname{div} \vec{\mathbf{F}} = 0, \tag{1}$$

where $\mathbf{U}$ contains the usual conservative variables and $\vec{\mathbf{F}} = \mathbf{F}_x \vec{i} + \mathbf{F}_y \vec{j} + \mathbf{F}_z \vec{k}$ is the inviscid flux. We will denote by an overhead arrow the vectors associated with the physical (Cartesian) coordinates in three dimensions. It turns out to be intriguing to write the flux $\vec{\mathbf{F}}$ as

$$\vec{\mathbf{F}} = \vec{\mathbf{F}}^{(c)} + \vec{\mathbf{P}} = \vec{m}\Psi + \vec{\mathbf{P}}, \tag{2}$$

where

$$\Psi = \begin{pmatrix} 1 \\ u \\ v \\ w \\ H \end{pmatrix}, \qquad \vec{\mathbf{P}} = \begin{pmatrix} 0 \\ p\vec{i} \\ p\vec{j} \\ p\vec{k} \\ 0 \end{pmatrix}. \tag{3}$$

The first term in $\vec{\mathbf{F}}$ is the *convective* flux $\vec{\mathbf{F}}^{(c)}$, indicating the convection of Ψ by the mass flux $\vec{\dot{m}}$ and the second term is the *pressure* flux $\vec{\mathbf{P}}$, containing nothing but the pressure.

The mass flux $\vec{\dot{m}}$ and pressure flux $\vec{\mathbf{P}}$, respectively, consist of three Cartesian components,

$$\vec{\dot{m}} = \dot{m}_x\vec{i} + \dot{m}_y\vec{j} + \dot{m}_z\vec{k} = \rho u\vec{i} + \rho v\vec{j} + \rho w\vec{k} = \rho\vec{V}, \tag{4}$$

and

$$\vec{\mathbf{P}} = \mathbf{P}_x\vec{i} + \mathbf{P}_y\vec{j} + \mathbf{P}_z\vec{k}; \qquad \mathbf{P}_x = \begin{pmatrix} 0 \\ p \\ 0 \\ 0 \\ 0 \end{pmatrix}, \quad \mathbf{P}_y = \begin{pmatrix} 0 \\ 0 \\ p \\ 0 \\ 0 \end{pmatrix}, \quad \mathbf{P}_z = \begin{pmatrix} 0 \\ 0 \\ 0 \\ p \\ 0 \end{pmatrix}. \tag{5}$$

Then we can further express the component fluxes in the directions x, y, and z in a unified form,

$$\mathbf{F}_i = \dot{m}_i\Psi + \mathbf{P}_i, \qquad i = x, y, z \tag{6}$$

and

$$\vec{\mathbf{F}} = (\dot{m}_x\Psi + \mathbf{P}_x)\vec{i} + (\dot{m}_y\Psi + \mathbf{P}_y)\vec{j} + (\dot{m}_z\Psi + \mathbf{P}_z)\vec{k}. \tag{7}$$

In a control volume, the mass flux $\dot{m}_n$ through a control surface having a unit normal vector $\vec{n} = (n_x, n_y, n_z)$ is given by

$$\dot{m}_n = \rho\vec{V}\cdot\vec{n} = n_x\dot{m}_x + n_y\dot{m}_y + n_z\dot{m}_z, \tag{8}$$

and the flux is the combination of the three component fluxes,

$$\mathbf{F}_n = \vec{\mathbf{F}}\cdot\vec{n} = n_x\mathbf{F}_x + n_y\mathbf{F}_y + n_z\mathbf{F}_z = \dot{m}_n\Psi + \mathbf{P}_n, \qquad \mathbf{P}_n = p\begin{pmatrix} 0 \\ n_x \\ n_y \\ n_z \\ 0 \end{pmatrix}. \tag{9}$$

Formally this equation looks the same as that along the coordinate direction, Eq. (6). Hence, at each control surface, the mass flux is treated in a one-dimensional fashion. At the

discrete level, this is all one needs to define for the flux at the interface in a finite volume. Hereafter, we will assume that this local orientation has been accomplished and the velocity vector (hence mass flux) decomposed into components normal and parallel to the surface vectors $\vec{n}$. Therefore, the subscripts n denoting the normal component will be dropped.

From the above equations, the principal quantities in $\mathbf{F}_n$ again are the convective flux and the pressure flux. The distinction of these two fluxes gives rise to the basis for the development of the AUSM-family schemes. The fact that a common mass flux $\dot{m}_n$ appears in all equations is rather clear in the above derivations at the continuum level. Since the mass flux is common to all equations, its effects will thus perpetuate to all variables. Hence, we submit that it is desirable to observe this fact at the discrete level as well when devising a new scheme. We note that several modern numerical schemes do not follow this criterion. While it is not necessary to follow this criterion, however, significant benefits can be realized otherwise. For example, the numerical dissipation term is scalar even for the system of equations; it is just as easy to add more conservation equations insofar as the numerical flux is concerned.

As a primary objective of this paper, we will demonstrate that the mass flux holds an important key in explaining certain catastrophic failings associated with existing schemes.

3. NUMERICAL MASS FLUXES

It is possible to write a numerical flux, which explicitly expresses a common mass flux in the general form

$$\mathbf{f}_{1/2} = \dot{m}^{+}_{1/2}\Psi_{\mathrm{L}} + \dot{m}^{-}_{1/2}\Psi_{\mathrm{R}} + \begin{pmatrix} 0 \\ p_{1/2}n_x \\ p_{1/2}n_y \\ p_{1/2}n_z \\ \delta \end{pmatrix}, \tag{10}$$

where the subscript n has been deleted as indicated above. The subscripts L and R are understood to mean the cell centers on either side of the interface at which the normal vector is assumed, for convenience, to point from L to R.

It must be noted that the flux expressed in the form of Eq. (10) implies that the numerical dissipation is of the scalar, rather than the matrix, form, because the same factors $\dot{m}^{\pm}_{1/2}$ are applied throughout for all conservation equations. This type of form however can not be done for the flux difference splitting schemes, like the Roe or Osher–Soloman splitting. The former encompasses many existing schemes, such as central differencing with artificial damping, and those to be discussed in this paper. The latter includes the Roe and Osher–Solomon schemes. A main theme of this paper is to show that the flux expressed in Eq. (10) has attractive properties which we will bring forth wherever appropriate.

The quantities $(\dot{m}^{+}_{1/2}, \dot{m}^{-}_{1/2})$ refer to the flux components normal to the interface of a discrete volume and are required to satisfy (see Corollary 1)

$$(\dot{m}^{+}_{1/2})(\dot{m}^{-}_{1/2}) \le 0. \tag{11}$$

In many schemes, both are mutually exclusive, i.e.,

$$(\dot{m}^+_{1/2})(\dot{m}^-_{1/2}) \equiv 0. \tag{12}$$

From the first element of Eq. (10), we have the expression of the mass flux

$$\dot{m}_{1/2} = \dot{m}^+_{1/2} + \dot{m}^-_{1/2}. \tag{13}$$

Here we call the readers' attention that in general $\dot{m}^\pm_{1/2} \neq (\dot{m}_{1/2} \pm |\dot{m}_{1/2}|)/2$; see Eqs. (29) and (33) for the Van Leer and HLLE schemes. Using Eq. (13), one can readily rewrite Eq. (10) as

$$\mathbf{f}_{1/2} = \frac{1}{2}\dot{m}_{1/2}(\Psi_\mathrm{L} + \Psi_\mathrm{R}) - \frac{1}{2}\mathcal{D}_m(\Psi_\mathrm{R} - \Psi_\mathrm{L}) + \begin{pmatrix} 0 \\ p_{1/2}n_x \\ p_{1/2}n_y \\ p_{1/2}n_z \\ \delta \end{pmatrix}, \tag{14}$$

where the dissipation term, $\mathcal{D}_m$, is defined as

$$\mathcal{D}_m = \dot{m}^+_{1/2} - \dot{m}^-_{1/2}. \tag{15}$$

This term is a scalar quantity, common to all equations, and is expected to be nonnegative in order to provide proper upwinding, thus ensuring stability. Hence the differences among the following schemes lie chiefly in the definitions of $\dot{m}^\pm_{1/2}$, $p_{1/2}$, and δ. The function δ is zero for the AUSM-family schemes and nonzero for the others.

Of all the existing numerical flux schemes, only those with the *scalar*, as opposed to *matrix*, dissipation term will yield a common mass flux. Thus, the AUSM-type, Van Leer-type [6, 7], HLLE [8], and CUSP [16, 21] schemes can be classified as the scalar upwind schemes. The Roe, Osher–Solomon, and improved versions of the HLLE schemes [9, 10] belong to the matrix upwind schemes.

In the next section we will examine the above schemes with focus on the mass flux, consequently leading to a new interpretation of them.

To facilitate the discussion, we first define the split functions

$$\mathcal{M}^\pm_{(1)}(M) = \frac{1}{2}(M \pm |M|), \tag{16}$$

$$\mathcal{M}^\pm_{(4,\beta)}(M) = \begin{cases} \mathcal{M}^\pm_{(1)}(M), & \text{if } |M| \geq 1, \\ \pm\frac{1}{4}(M \pm 1)^2 \pm \beta(M^2-1)^2; \ -1/16 \leq \beta \leq 1/2, & \text{otherwise,} \end{cases} \tag{17}$$

and

$$\mathcal{P}^\pm_{(5,\alpha)}(M) = \begin{cases} \frac{1}{M}\mathcal{M}^\pm_{(1)}(M), & \text{if } |M| \geq 1, \\ \frac{1}{4}(M \pm 1)^2(2 \mp M) \pm \alpha M(M^2-1)^2; \ -3/4 \leq \alpha \leq 3/16, & \text{otherwise.} \end{cases} \tag{18}$$

The numerals in the subscript of $\mathcal{M}^{\pm}_{(1)}$, $\mathcal{M}^{\pm}_{(4,\beta)}$, and $\mathcal{P}^{\pm}_{(5,\alpha)}$ indicate the degree of polynomials, while the range of parameters (α, β) is set to meet the monotonicity requirements. In practice, we set $\alpha = 3/16$ and $\beta = 1/8$.

AUSM$^+$ [11]

Let $M_{\rm L} = u_{n_{\rm L}}/a_{1/2}$ and $M_{\rm R} = u_{n_{\rm R}}/a_{1/2}$. Then we define

$$M_{1/2} = \mathcal{M}^{+}_{(4,\beta)}(M_{\rm L}) + \mathcal{M}^{-}_{(4,\beta)}(M_{\rm R}), \tag{19a}$$

$$M^{\pm}_{1/2} = \frac{1}{2}\big(M_{1/2} \pm |M_{1/2}|\big). \tag{19b}$$

$$\dot{m}^{+}_{1/2}(\mathbf{U}_{\rm L}, \mathbf{U}_{\rm R}) = \rho_{\rm L} a_{1/2} M^{+}_{1/2} = \rho_{\rm L} a_{1/2} \max\big(0, M_{1/2}\big), \tag{20a}$$

$$\dot{m}^{-}_{1/2}(\mathbf{U}_{\rm L}, \mathbf{U}_{\rm R}) = \rho_{\rm R} a_{1/2} M^{-}_{1/2} = \rho_{\rm R} a_{1/2} \min\big(0, M_{1/2}\big). \tag{20b}$$

Notice that a common speed of sound $a_{1/2} = a(\mathbf{U}_{\rm L}, \mathbf{U}_{\rm R})$ is used in the formulation. In [11], we give a special formula to define $a_{1/2}$ such that an exact shock capturing can be achieved for a stationary normal shock. Otherwise any averages between the L and R states should be appropriate.

Next the pressure at the interface is simply given by

$$p_{1/2} = \mathcal{P}^{+}_{(5,\alpha)}(M_{\rm L})\, p_{\rm L} + \mathcal{P}^{-}_{(5,\alpha)}(M_{\rm R})\, p_{\rm R}. \tag{21}$$

It is easy to show that a nonnegative $\mathcal{D}_m$ is obtained. Specifically,

$$\mathcal{D}_m = \mathrm{abs}\big(\dot{m}_{1/2}\big) = \big|\dot{m}_{1/2}\big| = a_{1/2}\big|M_{1/2}\big| \begin{cases} \rho_{\rm L}, & \text{if } M_{1/2} \geq 0, \\ \rho_{\rm R}, & \text{otherwise.} \end{cases} \tag{22}$$

It is noted that $M_{1/2}$ and $\dot{m}_{1/2}$ have the same sign because $\dot{m}^{+}_{1/2}\dot{m}^{-}_{1/2} \equiv 0$, $\Leftrightarrow$ $\dot{m}^{\pm}_{1/2} = (\dot{m}_{1/2} \pm |\dot{m}_{1/2}|)/2$. It makes no difference which variable of $(M_{1/2}, \dot{m}_{1/2})$ is used for switching in Eq. (22).

AUSMDV [2]

Let

$$M^{+}_{1/2}(\mathbf{U}_{\rm L}, \mathbf{U}_{\rm R}) = \big[\omega^{+}_{1/2}\mathcal{M}^{+}_{(4,\beta)}(M_{\rm L}) + \big(1 - \omega^{+}_{1/2}\big)\mathcal{M}^{+}_{(1)}(M_{\rm L})\big], \tag{23a}$$

$$M^{-}_{1/2}(\mathbf{U}_{\rm L}, \mathbf{U}_{\rm R}) = \big[\omega^{-}_{1/2}\mathcal{M}^{-}_{(4,\beta)}(M_{\rm R}) + \big(1 - \omega^{-}_{1/2}\big)\mathcal{M}^{-}_{(1)}(M_{\rm R})\big], \tag{23b}$$

together with the blending functions,

$$\omega^{+}_{1/2}(\mathbf{U}_{\rm L}, \mathbf{U}_{\rm R}) = \frac{2 f_{\rm L}}{f_{\rm L} + f_{\rm R}}, \qquad \omega^{-}_{1/2}(\mathbf{U}_{\rm L}, \mathbf{U}_{\rm R}) = \frac{2 f_{\rm R}}{f_{\rm L} + f_{\rm R}}, \quad f = p/\rho. \tag{23c}$$

We define

$$\dot{m}_{1/2} = a_{1/2}\big(\rho_{\rm L} M^{+}_{1/2} + \rho_{\rm R} M^{-}_{1/2}\big), \tag{24}$$

and

$$\dot{m}^+_{1/2} = \frac{1}{2}\big(\dot{m}_{1/2} + |\dot{m}_{1/2}|\big), \qquad \dot{m}^-_{1/2} = \dot{m}_{1/2} - \dot{m}^+_{1/2}. \tag{25}$$

The pressure flux is defined identically as in Eq. (21). Also the dissipation is

$$\mathcal{D}_m = \mathrm{abs}\big(\dot{m}_{1/2}\big) = |\dot{m}_{1/2}| = a_{1/2}\big|\big(\rho_{\mathrm{L}} M^+_{1/2} + \rho_{\mathrm{R}} M^-_{1/2}\big)\big|. \tag{26}$$

It is noted that the dissipation $\mathcal{D}_m$ for the AUSM$^+$ and that for the AUSMDV turn out to have the same form, i.e., $|\dot{m}_{1/2}|$, but they differ in the appearance of ρ_{L} and ρ_{R} and that $M^+_{1/2}M^-_{1/2} = 0, \forall M$ for AUSM$^+$, but $\neq 0$, as $|M| < 1$ for AUSMDV. If in AUSMDV, $\omega^{\pm}$ are constant, then $M^+_{1/2}(M^-_{1/2})$ depends on $\mathbf{U}_{\mathrm{L}}(\mathbf{U}_{\mathrm{R}})$ alone. As a result, the mass flux given in Eq. (24) reduces to the form of the conventional flux-vector type splittings,[1] resulting in the smearing of contact discontinuities. Allowing that $\omega^{\pm}$ varies with flow variables, the AUSMDV is made to be accurate for capturing contact discontinuities. This point will be discussed in detail later.

Van Leer [6]

In the Van Leer scheme, we use the local speed of sound, a_{L} or a_{R}, to define Mach numbers,

$$M_{\mathrm{L}} = u_{n_{\mathrm{L}}}/a_{\mathrm{L}}, \qquad M_{\mathrm{R}} = u_{n_{\mathrm{R}}}/a_{\mathrm{R}}. \tag{27}$$

The split Mach numbers and pressure are those in Eqs. (17) and (18) by setting $\alpha = \beta = 0$, hence reduced in the degree of polynomials:

$$\mathcal{M}^+_{(2)} \equiv \mathcal{M}^{\pm}_{(4,\beta=0)}, \qquad \mathcal{P}^{\pm}_{(3)} \equiv \mathcal{P}^{\pm}_{(5,\alpha=0)} = \pm(2 \mp M)\mathcal{M}^{\pm}_{(2)}. \tag{28}$$

Then, one can readily find in Eq. (10) the relationships

$$\dot{m}^+_{1/2}(\mathbf{U}_{\mathrm{L}}) = \rho_{\mathrm{L}} a_{\mathrm{L}} \mathcal{M}^+_{(2)}(M_{\mathrm{L}}), \tag{29a}$$

$$\dot{m}^-_{1/2}(\mathbf{U}_{\mathrm{R}}) = \rho_{\mathrm{R}} a_{\mathrm{R}} \mathcal{M}^-_{(2)}(M_{\mathrm{R}}), \tag{29b}$$

$$p_{1/2} = \mathcal{P}^+_{(3)}(M_{\mathrm{L}})\, p_{\mathrm{L}} + \mathcal{P}^-_{(3)}(M_{\mathrm{R}})\, p_{\mathrm{R}}, \tag{30}$$

and

$$\delta = -\frac{\gamma}{\gamma+1}\big[\big(a\mathcal{M}^+_{(2)}\mathcal{M}^-_{(2)}p\big)_{\mathrm{R}} - \big(a\mathcal{M}^+_{(2)}\mathcal{M}^-_{(2)}p\big)_{\mathrm{L}}\big]. \tag{31}$$

The higher degree polynomials given in Eqs. (17) and (18) can be used as well. The Hänel modification [7] for the energy flux is obtained when δ is set to zero, leading to improved prediction of temperature profile in the boundary layer.

[1] This is true only for the mass flux, not the momentum and energy fluxes, because Eq. (25) is introduced in the AUSMDV scheme before using Eq. (10).

Notice that the split mass fluxes, $\dot{m}^{\pm}_{1/2}$ in Eq. (29), depend on only one of the states, i.e., either L or R, unlike the previous two schemes in which both states appear.

The dissipation $\mathcal{D}_m$ becomes

$$\mathcal{D}_m = \dot{m}^{+}_{1/2} - \dot{m}^{-}_{1/2} = \rho_{\mathrm{L}} a_{\mathrm{L}} \mathcal{M}^{+}_{(2)}(M_{\mathrm{L}}) - \rho_{\mathrm{R}} a_{\mathrm{R}} \mathcal{M}^{-}_{(2)}(M_{\mathrm{R}}) \tag{32}$$

and $\dot{m}^{+}_{1/2}\dot{m}^{-}_{1/2} \neq 0$ when $|M| < 1$.

HLLE [8]

We can rewrite the HLLE scheme in the form of Eq. (10) by setting

$$\dot{m}^{+}_{1/2}(\mathbf{U}_{\mathrm{L}}, \mathbf{U}_{\mathrm{R}}) = \rho_{\mathrm{L}}\left(u_{n_{\mathrm{L}}} - b^{-}\right)\frac{b^{+}}{b^{+} - b^{-}}, \tag{33a}$$

$$\dot{m}^{-}_{1/2}(\mathbf{U}_{\mathrm{L}}, \mathbf{U}_{\mathrm{R}}) = \rho_{\mathrm{R}}\left(u_{n_{\mathrm{R}}} - b^{+}\right)\frac{-b^{-}}{b^{+} - b^{-}}, \tag{33b}$$

$$p_{1/2} = \frac{b^{+}}{b^{+} - b^{-}} p_{\mathrm{L}} + \frac{-b^{-}}{b^{+} - b^{-}} p_{\mathrm{R}}, \tag{34}$$

and

$$\delta = -\frac{b^{+}b^{-}}{b^{+} - b^{-}}(p_{\mathrm{R}} - p_{\mathrm{L}}). \tag{35}$$

The quantities $b^{\pm}$ are the speeds used for representing the right- and left-running waves defined as follows:

$$b^{+} = \max(0, b_{\mathrm{R}}), \qquad b_{\mathrm{R}} = \max\left(\hat{u}_n + \hat{a}, u_{n_{\mathrm{R}}} + a_{\mathrm{R}}\right), \tag{36a}$$

$$b^{-} = \min(0, b_{\mathrm{L}}), \qquad b_{\mathrm{L}} = \min\left(\hat{u}_n - \hat{a}, u_{n_{\mathrm{L}}} - a_{\mathrm{L}}\right). \tag{36b}$$

The quantities denoted by $\hat{}$ are evaluated by the Roe averages. Some variations have been proposed in the literatures, but they do not differ in essence.

The interpretation of the HLLE scheme in the above framework is quite interesting and to the author's knowledge it has not been given in the literature elsewhere. The weightings in the pressure mass fluxes are the simplest form, based on the "positive" and "negative" portion of the widest wave angle possible in $(\mathbf{U}_{\mathrm{L}}, \mathbf{U}_{\mathrm{R}})$. In fact, one might further interpret the HLLE splitting in terms of Mach number and pressure splittings as

$$\mathcal{P}^{+}_{\mathrm{HLLE}} = \frac{\pm b^{\pm}}{b^{+} - b^{-}}, \qquad \mathcal{P}^{+}_{\mathrm{HLLE}} + \mathcal{P}^{-}_{\mathrm{HLLE}} = 1, \tag{37}$$

and

$$\mathcal{M}^{+}_{\mathrm{HLLE}} = (M_{\mathrm{L}} - b^{-}/a_{\mathrm{L}})\mathcal{P}^{+}_{\mathrm{HLLE}} \geq 0, \qquad \mathcal{M}^{-}_{\mathrm{HLLE}} = (M_{\mathrm{R}} - b^{+}/a_{\mathrm{R}})\mathcal{P}^{-}_{\mathrm{HLLE}} \leq 0. \tag{38}$$

The split mass and pressure fluxes appear to behave like a first-degree polynomial in $(M \pm 1)$ as $b^{+} > 0$ and $b^{-} < 0$, leading to nondifferentiability at the transition points. As

in the Van Leer scheme in Eq. (28), the split Mach numbers and pressures are related in a simple fashion.

Interestingly, we can rewrite the HLLE flux in a form similar to that of the conventional flux vector splitting,

$$\dot{m}^+_{1/2} = \rho_L a_L \mathcal{M}^+_{\text{HLLE}}, \tag{39a}$$

$$\dot{m}^-_{1/2} = \rho_R a_R \mathcal{M}^-_{\text{HLLE}}, \tag{39b}$$

and

$$p_{1/2} = \mathcal{P}^+_{\text{HLLE}} p_L + \mathcal{P}^-_{\text{HLLE}} p_R. \tag{40}$$

However, $\mathcal{M}^\pm_{\text{HLLE}}$ and $\mathcal{P}^\pm_{\text{HLLE}}$ are functions of both states, i.e., $(\mathbf{U}_L, \mathbf{U}_R)$.

In summary, some observations concerning the above-listed schemes are in order.

1. All schemes involve automatic switching from the condition for $|M| < 1$ to that for $|M| \geq 1$ and these switchings are determined by the wave speeds associated with nonlinear fields $(M \pm 1)$.

2. The split mass fluxes $\dot{m}^\pm$ in all but the Van Leer schemes are a function of both the L and R states.

3. The quantity δ involves the mixing of both $+$ and $-$ wave speeds for the Van Leer and HLLE schemes.

4. Most importantly, the mass flux $\dot{m}_{1/2}$ appears throughout the entire system of equations and is the key element in defining the numerical flux $\mathbf{f}_{1/2}$.

COROLLARY 1. *The split mass fluxes of all schemes listed above possess the nonnegative and nonpositive properties*

$$\dot{m}^+_{1/2} \geq 0 \qquad \textit{and} \qquad \dot{m}^-_{1/2} \leq 0. \tag{41}$$

Then the dissipation coefficient $\mathcal{D}_m$ satisfies the positivity property

$$\mathcal{D}_m \geq 0. \tag{42}$$

Proof. The proof for the AUSM$^+$, AUSMDV, and Van Leer schemes is obvious by inspection. To prove them for the HLLE scheme, we just need to utilize the Corollary established in the Appendix and the facts $b^+ \geq 0$ and $b^- \leq 0$.

In the remainder of this paper, analysis of the mass flux will be carried out. Consequently, we develop a criterion useful for the purpose of designing the mass flux. And we will demonstrate how some prominent upwind schemes encounter difficulties when they do not satisfy this criterion.

We can write the mass flux in the most general form

$$\dot{m}_{1/2} = \langle \dot{m} \rangle - \frac{1}{2}\mathcal{D}(\mathbf{U}_L, \mathbf{U}_R), \tag{43}$$

where $\langle \dot{m} \rangle$ is a sort of centrally weighted average. The simplest form is

$$\langle \dot{m} \rangle = \frac{1}{2}[(\rho u_n)_L + (\rho u_n)_R] = \frac{1}{2}(\dot{m}_L + \dot{m}_R). \tag{44}$$

The dissipative term $\mathcal{D}(\mathbf{U}_\mathrm{L}, \mathbf{U}_\mathrm{R})$ can be further expanded in terms of differences of primitive variables $\mathbf{U} = (\rho, \vec{u}, p)^T$, $\vec{u} = (u_1, u_2, u_3)$, as

$$\mathcal{D} = \mathcal{D}^{(\rho)}(\bar{\mathbf{U}})\Delta\rho + \sum_l \mathcal{D}^{(u_l)}(\bar{\mathbf{U}})\Delta u_l + \mathcal{D}^{(p)}(\bar{\mathbf{U}})\Delta p, \tag{45}$$

where $\bar{\mathbf{U}}(\mathbf{U}_\mathrm{L}, \mathbf{U}_\mathrm{R})$ are some mean quantities, whose precise definitions are immaterial for the present discussion. The difference operator is $\Delta(\bullet) = (\bullet)_\mathrm{R} - (\bullet)_\mathrm{L}$.

Needless to say, different schemes will have different representations for each individual element in $\mathcal{D}$ and as such they contribute to a variety of numerical behaviors. In what follows, we shall give mass flux formulas for various schemes, including those given above. By substituting the functions, $\dot{m}^{\pm}_{1/2}$, we get the corresponding expression for $\langle \dot{m} \rangle$ and $\mathcal{D}$.

For the AUSM$^+$ flux,

$$\begin{aligned} \langle \dot{m} \rangle &= \tfrac{1}{2}(\rho_j + \rho_{j+1})u_{1/2}, \qquad u_{1/2} = a_{1/2}M_{1/2}, \\ \mathcal{D}^{(\rho)} &= |u_{1/2}|, \\ \mathcal{D}^{(p)} &= 0. \end{aligned} \tag{46}$$

For the AUSMDV flux,

$$\begin{aligned} &\langle \dot{m} \rangle = \tfrac{1}{2}(\dot{m}_\mathrm{L} + \dot{m}_\mathrm{R}), && \dot{m} = \rho u_n, \\ &\mathcal{D}^{(\rho)} = \tfrac{1}{2}(|u_\mathrm{L}| + |u_\mathrm{R}|), \\ &\mathcal{D}^{(p)} = 2a_{1/2}(g_\mathrm{L} + g_\mathrm{R}) \Big/ \left[\left(\frac{p}{\rho}\right)_\mathrm{L} + \left(\frac{p}{\rho}\right)_\mathrm{R} \right], && g(M) = \mathcal{M}^+_{(4,\beta)} - \mathcal{M}^+_{(1)} \geq 0. \end{aligned} \tag{47}$$

For the Van Leer flux,

$$\begin{aligned} \langle \dot{m} \rangle &= \tfrac{1}{2}\big(\rho_\mathrm{L} + \rho_\mathrm{R}\big)\big(a_\mathrm{L}\mathcal{M}^+_{(2)}(M_\mathrm{L}) + a_\mathrm{R}\mathcal{M}^-_{(2)}(M_\mathrm{R})\big), \\ \mathcal{D}^{(\rho)} &= a_\mathrm{L}\mathcal{M}^+_{(2)}(M_\mathrm{L}) - a_\mathrm{R}\mathcal{M}^-_{(2)}(M_\mathrm{R}), \\ \mathcal{D}^{(p)} &= 0. \end{aligned} \tag{48}$$

For the HLLE flux,

$$\begin{aligned} \langle \dot{m} \rangle &= [b^+(\rho u_n)_\mathrm{L} - b^-(\rho u_n)_\mathrm{R}]/(b^+ - b^-), \\ \mathcal{D}^{(\rho)} &= -2b^+b^-/(b^+ - b^-), \\ \mathcal{D}^{(p)} &= 0. \end{aligned} \tag{49}$$

The coefficients $\mathcal{D}^{(u_l)}$ in the above schemes are somewhat more involved than $\mathcal{D}^{(\rho)}$ and $\mathcal{D}^{(p)}$, but fortunately they are not important within the scope of the present investigation.

Similarly, we can write the dissipation coefficients in $\dot{m}$ for the Roe schemes,

$$\begin{aligned} \langle \dot{m} \rangle &= (\dot{m}_\mathrm{L} + \dot{m}_\mathrm{R})/2, \qquad \dot{m} = \rho u_n \\ \mathcal{D}^{(\rho)} &= |\lambda_2|, \\ \mathcal{D}^{(p)} &= (|\lambda_1| + |\lambda_3| - 2|\lambda_2|)/2a^2, \end{aligned} \tag{50}$$

where $\{\lambda_k, k=1,2,3\} = \{u_n - a, u_n, u_n + a\}$ and the quantities are understood to be evaluated using the usual Roe averages. Note that the Roe flux does not fit in the expression in Eq. (10). Hence the mass flux is only used in the continuity equation.

Remark. We observe the following interesting properties pertaining to the above-mentioned schemes. For any $[\mathbf{U}_L, \mathbf{U}_R]$,

$$\begin{aligned} &(1) \quad \mathcal{D}^{(\rho)} \geq 0, && \text{for all schemes,} \\ &(2) \quad \mathcal{D}^{(p)} \begin{cases} \equiv 0, \\ \geq 0, \end{cases} && \begin{matrix} \text{AUSM}^+, \text{ Van Leer, and HLLE only} \\ \text{otherwise.} \end{matrix} \end{aligned} \tag{51}$$

We stress that this way of classifying the dissipation terms gives an interesting approach to studying flux functions. Specifically, it provides a tool for discriminatingly detecting causes of failures, because each individual term can be probed pathologically. This will become clear as we discuss Lemma 1 below and the Conjecture to be given in Section 4.

LEMMA 1. *The exact solution of the Riemann problem for a contact discontinuity moving with speed u_c requires that*

$$\mathcal{D}^{(\rho)} = |u_c| \qquad as\ (u, p)_L = (u, p)_R = (u_c, p) \quad and \quad \rho_L \neq \rho_R. \tag{52}$$

This is shown to be a sufficient and necessary condition. This result is useful for checking the accuracy of numerical flux functions and it can provide us with a new insight about their behavior.

A special case is the stationary contact discontinuity where $u_c = 0$. We find all but the Van Leer and HLLE schemes listed above yield the exact result, $\mathcal{D}^{(\rho)} = 0$. This is the argument that the schemes do not satisfy this condition are not suitable for accurate resolution of viscous layers because they behave like a contact discontinuity. Figure 1 displays the 2D viscous solutions of a $M_\infty = 6$ flow over a circular cylinder by the Van Leer, HLLE, AUSMDV, and AUSM$^+$ schemes, confirming the above statement. Both the Van Leer and HLLE solutions yield a diffused, thicker boundary layer as evident in the temperature profile and a much lower enthalpy (respectively 5.21 and 4.90) at the stagnation point. These are the indication of excessive numerical dissipation. The AUSMDV and AUSM$^+$ solutions, on the other hand, predict a thinner boundary layer and give the value of the stagnation enthalpy (12.8) that is already grid independent (to the third decimal point). Both solutions are nearly identical, except in the neighborhood of the stagnation point. The nature of numerical diffusion also can be seen in the Stanton number distribution in the figure. Thus, a scheme's ability to accurately resolve a contact discontinuity is an important criterion and Lemma 1 is useful in this sense.

In what follows, we will primarily focus on the schemes that will at minimum preserve the stationary contact discontinuity. These are the schemes of Roe [4], Osher and Solomon [5], modified HLLE [8], AUSM$^+$, and AUSMDV [2, 11]. It can be checked easily that they all satisfy Eq. (52). We note that while the original AUSM scheme [12] results in $\mathcal{D}^{(\rho)} = 0$ for a stationary contact, it however does not satisfy (52) for a moving contact. The consequences are what is seen in Fig. 2, in which a glitch clearly shows up in a slowly moving contact discontinuity. The dramatic improvement by the AUSM$^+$ scheme is due to the use of a common speed of sound $a_{1/2}$.

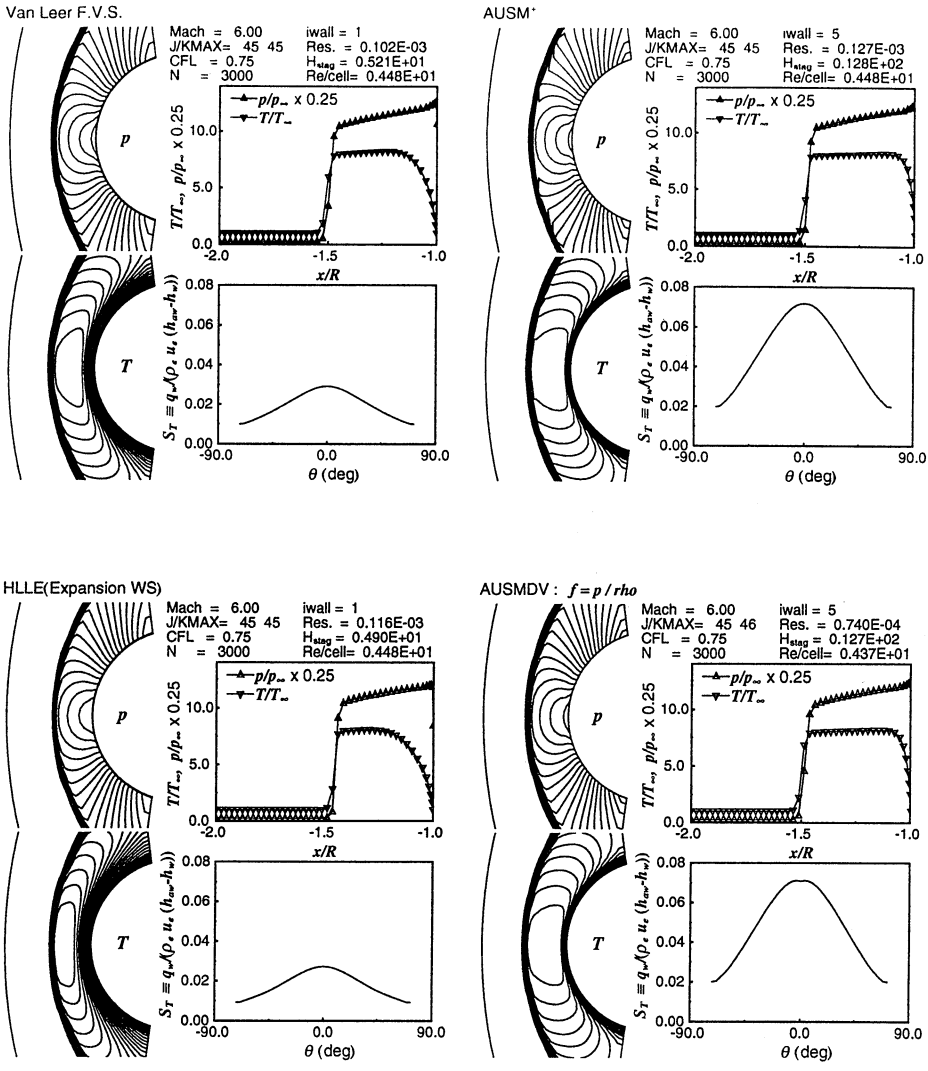

FIG. 1. Viscous solutions of a $M_\infty = 6$ flow over a circular cylinder: comparison of calculations using the Van Leer, HLLE, AUSM$^+$, and AUSMDV schemes.

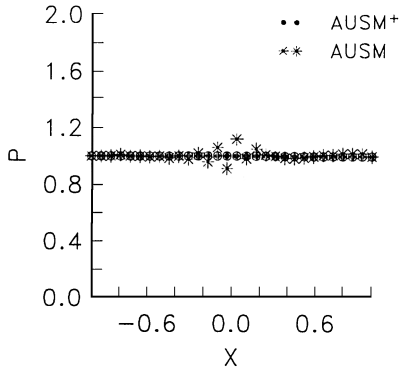

FIG. 2. Slowly moving contact; comparison of AUSM and AUSM$^+$ solutions.

The concept of using the common speed of sound turns out to be useful also in the formulation of the AUSMDV scheme. It is a necessary ingredient to blend two Mach number distributions, Eqs. (23), such that stationary and moving contact discontinuities can be accurately predicted. A sufficient condition for the AUSMDV scheme to ensure Lemma 1 is found to be

$$\rho_L \omega^+_{1/2} = \rho_R \omega^-_{1/2}, \qquad \forall \beta. \tag{53}$$

Hence, many forms are possible for $\omega^{\pm}$ so long as the above condition is met. A symmetry form is proposed in Eq. (23c) with $f = p/\rho$. Next we will consider the performance of each mass flux, specifically with respect to the odd–even decoupling and the carbuncle phenomenon.

4. SHOCK INSTABILITY: A MULTIDIMENSIONAL PROBLEM

The catastrophic failings in the supersonic blunt body flow (dubbed the carbuncle phenomenon) and the odd–even grid perturbation problem have been reported in [17] and later investigated by several authors [13, 18, 19, 22]. These seemingly benign problems prove to be rather daunting for many upwind schemes, including the exact Riemann solver by Godunov [1] and the approximate ones by Roe [4] and Osher and Solomon [5]. Even, to our disappointment, the recent HUS [14], AUSMDV [2], and LDFSS [19] schemes cannot escape the difficulty.

In [2], we suggested that these type of failings can be described as a *transverse* numerical instability associated with the shock wave. We called it the *shock instability* because a small disturbance near the shock results in a rather rapid amplification. It is a multidimensional problem in which disturbances communicate, feed into each other, and grow in multidimensions. Hence, multidimensional analysis is necessary. In a linear analysis, Quirk [13] pointed out that the pressure perturbation could feed into the density perturbation, resulting in a linear growth. He suggested the use of combined fluxes in the code so that one flux scheme is favored over another locally. In [17, 18, 22], attempts to rectify the Roe scheme were focused on modifying the eigenvalues in the form of entropy fix. They all involve a modification/contribution resulting from a multidimensional consideration. And clearly there is more than one way to fix the problem. However, with these fixes, one is still left with the question of *what* causes this shock instability—why are some flux schemes free from it? What can one learn from the finding in order to help development of future flux schemes? These are the main objectives of the present paper.

First, we give the following definition.

DEFINITION. A scheme is called shock stable if it does not yield an amplification of disturbances at the shock.

It must be noted that the occurrence of the carbuncle phenomenon for a shock-unstable scheme is sensitive to several factors, such as irregularity and aspect ratio of a grid, boundary condition, and shock strength. In other words, in the case of a shock-unstable scheme, change in grid distribution or order of accuracy may add just enough dissipation to suppress the instability. Our experiences indicate that the grid symmetry for the blunt body problem makes it easier to trigger the carbuncle phenomenon. Nevertheless, a shock-unstable scheme will eventually lead to shock instability if subject to sufficient perturbations. Some perturbations are just on the order of double precision roundoff [22]. It is also important to

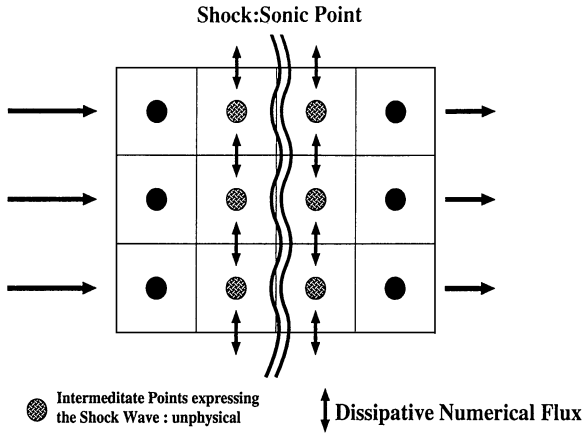

FIG. 3. Suggested scenario of carbuncle phenomenon and the proposed fix.

remember that shock instability, by definition, requires the presence of a shock. Hence its strength is necessarily finite, albeit possibly small.

We suggested in [2] the following heuristic explanation to the events taking place during the development of the carbuncle phenomenon. When the shock wave is captured by a shock-capturing scheme, intermediate (numerical) points are added to express a shock position numerically; see Fig. 3. In the 1-D case, this is not a problem for most existing schemes. But when the schemes are applied to a multidimensional calculation, these intermediate points exchange information with the neighbors, which are also intermediate shock points. We suspect that an unstable system is developed, involving the exchange of information between these nonphysical states, which eventually leads to a catastrophic carbuncle instability. If this is true, then a mechanism needed to stabilize the shock by some "appropriate"[2] schemes becomes obvious. The idea behind this is that one wants to choose a substitute scheme that can disrupt the communication of disturbances from one direction to another. We call this procedure "shock fix," which we shall prescribe as follows.

Shock Fix

1. Set the shock-point (also sonic-point) flag,

$$S_{\xi,j} = S_{\xi,j+1} = 1, \qquad \text{if } \begin{cases} u_j - a_j > 0 \quad \text{and} \quad u_{j+1} - a_{j+1} < 0, \quad \text{or} \\ u_j + a_j > 0 \quad \text{and} \quad u_{j+1} + a_{j+1} < 0, \end{cases} \tag{54}$$

between grid point j and $j+1$ in the ξ-direction. The same procedure is also done for the (η, ζ) directions.

2. Modify the numerical flux $\mathbf{f}_{\xi_{1/2}}$ in the ξ-direction by a dissipative scheme if a shock-point in the *transverse* directions is detected. That is,

$$\mathbf{f}_{\xi_{1/2}} = \begin{cases} \text{dissipative scheme;} & \text{if } (S_{\eta,j} + S_{\eta,j+1} + S_{\zeta,j} + S_{\zeta,j+1}) \geq 1; \\ \text{unmodified;} & \text{otherwise.} \end{cases} \tag{55}$$

[2]A general answer to the question of what is "appropriate" is the subject of this paper, but at this juncture we shall simply suggest a dissipative counterpart of the underlying scheme.

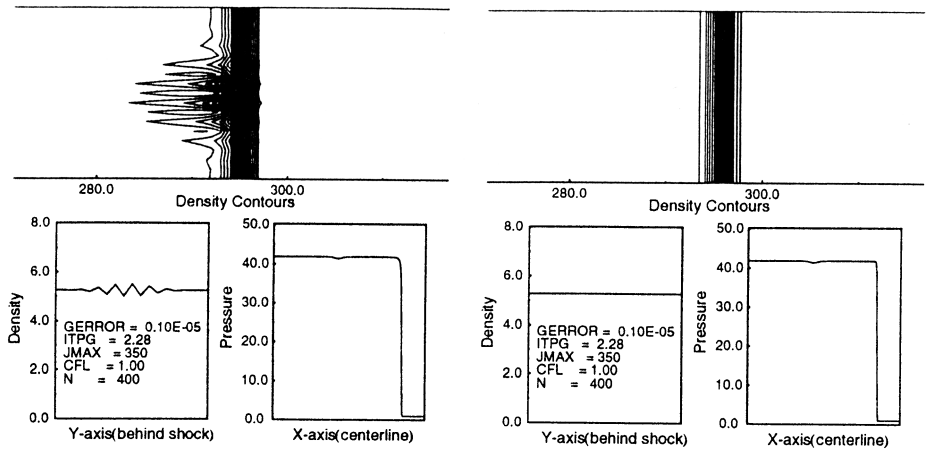

FIG. 4. Odd–even grid perturbation problem by AUSMDV, without and with shock fix, Eqs. (54)–(55).

This shock fix is general and can be applied to other numerical fluxes as well, such as the Roe, Osher–Solomon, and HUS methods. For the AUSMDV, we employ Hänel's FVS scheme [7], because it is dissipative enough and conserves the total enthalpy for steady flows. It is noted that the numerical Hänel's flux is now modified to include the common speed of sound, thereby maintaining the contact-capturing capability. The numerical fluxes in other directions are calculated in a similar way.

Figure 4 shows that the carbuncle phenomenon predicted by the unmodified AUSMDV scheme is now completely removed with this proposed shock fix. More interestingly, the shock fix can be also applied to Roe's approximate Riemann solver, for which the HLLE scheme is considered to be a dissipative partner scheme. The result by the Roe scheme together with the shock fix via the HLLE scheme is shown in Fig. 5, where the instability is again totally eliminated. This indicates the validity of the proposed cure for the carbuncle phenomenon, and the above results seem to support our belief about the dynamics of the instability process. We remark that this method does not use the pressure gradient for sensing shock waves because the pressure gradient does not always provide accurate information to distinguish a shock wave from a compressive wave.

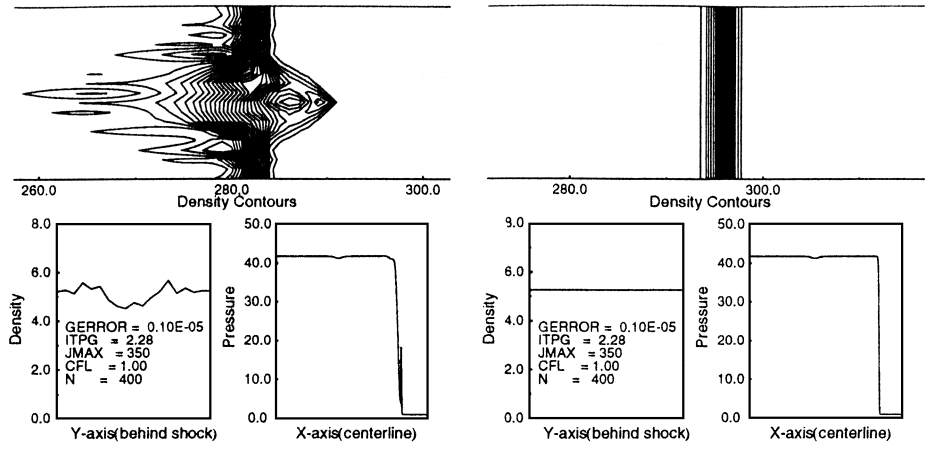

FIG. 5. Odd–even grid perturbation problem by the Roe scheme, without and with shock fix, Eqs. (54)–(55).

Despite the success of this shock fix, it is still not so desirable to have, even though it may be invented on the basis of sound reasoning. It needs an ad hoc detection and it might fail when the problem involves interactions of complex features. Moreover, we are still left with no clue as to why it works. In particular, the fact that the so-called "dissipative scheme" to which the basic scheme is switched works was discovered by playing a hunch, because adding more dissipation seems to be a good insurance policy. On the other hand, low diffusion schemes, such as AUSM or AUSM$^+$, have also been known to be free from these shock instabilities. So it is clear that adding dissipation is not necessarily a correct approach. Hence the puzzle remains to be unraveled.

In what follows we shall describe the attempt to identify the mechanism or the root of the problem—specifically the terms in the numerical fluxes that are responsible for these failings. With the mechanism understood, we will have a criterion that can specifically suggest which are the alternative replacement schemes in the shock fix.

Further study suggests that the term $\mathcal{D}^{(p)}$ in the mass flux plays a key role in causing the shock instability. As a result, we have reached the following conjecture.

CONJECTURE. *The condition $\mathcal{D}^{(p)} \neq 0, \forall M$, in the mass flux is necessary for a scheme to develop, as t increases, the shock instability as manifested by the odd–even decoupling and carbuncle phenomena. On the other hand, the condition $\mathcal{D}^{(p)} = 0, \forall M$, is sufficient for a scheme to prevent the shock instability from occurring.*

This conjecture immediately leads to the following result, according to the definition of a shock-stable scheme.

LEMMA 2. *A scheme having the property $\mathcal{D}^{(p)} = 0$ in the mass flux is a shock-stable scheme.*

A rigorous proof for the Conjecture is difficult, if not impossible. But a heuristic argument for a system involving a set of simplifying assumptions can be constructed and leads to the result that the amplification factor is greater than unity, thus growth of disturbances. In [13], Quirk gave a one-dimensional analysis showing the effect of pressure perturbation to the density under the assumptions of no velocity perturbations. However, there was still no clue specifically as to which term or flux was responsible for the anomalies.

Since a more general analysis has not yet been developed, we shall resort to the numerical proof with evidence to substantiate the validity of the condition and counter-prove it by modifying those schemes afflicted with the instability in such a way that they have $\mathcal{D}^{(p)} = 0, \forall M$.

Among the schemes that satisfy Lemma 1, AUSM$^+$ (original AUSM is of its special case) is the only scheme in its original form that gives rise to $\mathcal{D}^{(p)} = 0, \forall M$, while the AUSMDV, Roe schemes (as shown above), and others yield nonvanishing $\mathcal{D}^{(p)}$ when $|M| < 1$. For Example, the Roe splitting in (50) becomes

$$\mathcal{D}^{(p)} = \begin{cases} 0, & \text{if } |M| \geq 1, \\ (1 - |M|)/a, & \text{otherwise.} \end{cases} \tag{56}$$

While the expression of $\mathcal{D}^{(p)}$ for the other schemes (such as AUSMDV in Eq. (47)) may be more complicated, the details are not essential for the discussion of shock instability. Most important of all is to recognize whether the term $\mathcal{D}^{(p)}$ exists or not. A summary of the pressure coefficient of various popular shock capturing schemes is presented in Table I,

TABLE I
Summary of $\mathcal{D}^{(p)}$ and Shock Instability

Scheme	$\mathcal{D}^{(p)}=0$	Shock instability	Lemma 1
AUSM$^+$	Yes	No	Yes
Van Leer	Yes	No	No
HLLE	Yes	No	No
AUSMDV ($f=p/\rho$)	No	Yes	Yes
AUSMDV ($f=1/\rho$)	Yes	No	Yes
HUS	No	Yes	Yes
Roe	No	Yes	Yes
Osher-Solomon	No	Yes	Yes
HLLEM	No	Yes	Yes
AUSM$^+$-R	No	Yes	Yes
CUSP	Yes	No	Yes/no[a]

[a] This depends on which version is used [21].

along with a column indicating shock instability. This clearly displays the close correlation of the role of $\mathcal{D}^{(p)}$ term and the occurrence of the shock instability. The AUSM$^+$, Van Leer, and HLLE schemes are the only ones listed in the table that are free of the anomalies. And among these three, the AUSM$^+$ is the only one yielding the least dissipation for the viscous calculation (recall Fig. 1), via obeying Lemma 1. More strikingly, there are many more schemes that follow Lemma 1, but give $\mathcal{D}^{(p)}\neq 0$ and are afflicted with the shock instability.

Notice that in the framework of the AUSM schemes the only difference between AUSM$^+$ and AUSMDV is in the definition of the mass flux $\dot{m}$ (see Eqs. (20) and (23)–(24)). Thus, it is natural to believe that the mass flux in Eq. (10) can be alternatively substituted with the mass flux in the Roe scheme, as suggested by Shima and Jounouchi [15], denoted here as AUSM$^+$-R, for it falls in the form of the AUSM scheme.

We display the Mach contours in Fig. 6 for the odd–even grid perturbation problem. It is evident that the Conjecture is confirmed by the fact that the AUSM$^+$ predicts the correct solution and the AUSMDV, Roe, and AUSM$^+$-R are afflicted with anomalies. Conversely, if these schemes are modified in such a way that $\mathcal{D}^{(p)}=0, \forall M$, then the instability is now completely gone, as is evident in the figures. This trick is achieved by fiddling with the linear field, i.e.,

$$|\lambda_2| = \max(a, |u|). \tag{57}$$

In other words, the *linear* field now is propagated with the speed of sound as $|M|<1$, instead of the fluid speed. This is in contrast to the HLLE scheme in which the largest values are adopted for the *nonlinear* fields. We must note that this shock instability cannot be remedied in the Roe flux by tuning the entropy fix alone, because the fix is applied in the contribution associated with the nonlinear field, while the root really lies in the linear field. We must also point out that this modification unfortunately fouls up the property in Lemma 1 and thus is not suitable for the viscous solution. The modification in Eq. (57) is intended only to support the Conjecture concerning the root of the shock instability. We shall call this the modified Roe scheme, denoted Roe_{mod} in the figure caption.

The original blending function in the AUSMDV scheme is chosen by including the pressure effect, which inadvertently leads to a nonvanishing $\mathcal{D}^{(p)}$, thereby resulting in shock

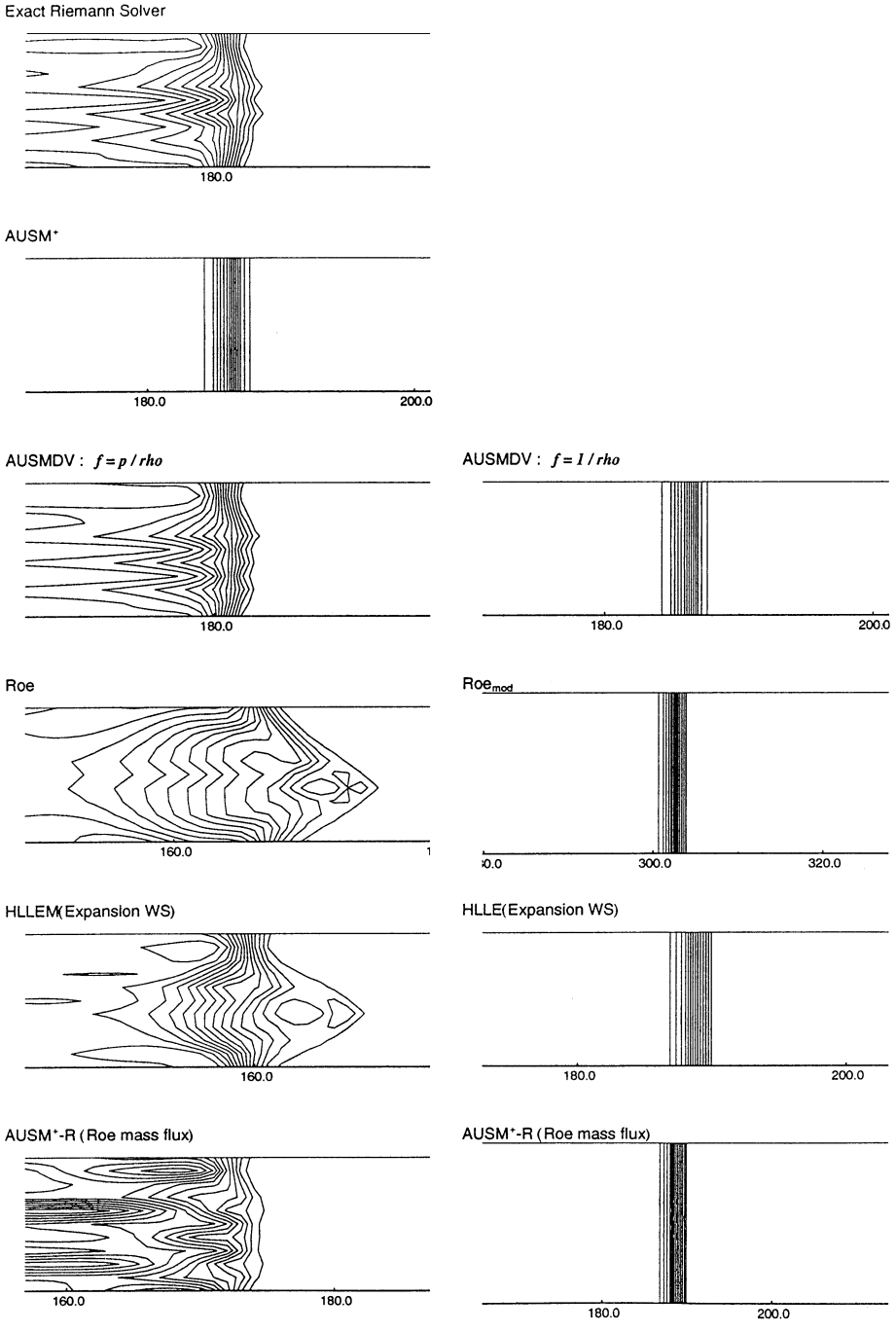

FIG. 6. Odd–even grid perturbation problem. Left, original schemes; right, modification with $\mathcal{D}^{(p)} = 0$.

instability. Fortunately, this can be easily corrected by retaining only the density effect, without sacrificing the accurate capturing of the contact discontinuity. This is achieved by defining

$$f = 1/\rho, \tag{58}$$

instead of $f = p/\rho$ in Eq. (23) (also denoted in the caption of Fig. 6), while Eq. (53) still holds.

The modified HLLE (or HLLEM) scheme is also designed to reduce the numerical dissipation for accurately resolving the contact discontinuity, by inserting a term resulting from the linear field of the Roe scheme. In 1D, it is given by

$$\mathbf{f}_{\mathrm{HLLEM}} = \mathbf{f}_{\mathrm{HLLE}} - \frac{b^+ b^-}{b^+ - b^-}\hat{\delta}_2 \hat{\alpha}_2 \hat{\mathbf{R}}_2. \tag{59}$$

The variables in the added term are

$$\hat{\delta}_2 = \frac{\hat{a}}{\hat{a} + \bar{u}}, \qquad \bar{u} = \frac{1}{2}(b_{\mathrm{L}} + b_{\mathrm{R}}), \tag{60a}$$

where $\hat{\mathbf{R}}_i$ $(i = 1, 2, 3)$ are the right eigenvectors of Jacobian $\frac{\partial \mathbf{F}}{\partial \mathbf{U}}$, and $\hat{\alpha}_2$ is the coefficient associated with the linear field in the expansion of $\mathbf{U}_{\mathrm{R}} - \mathbf{U}_{\mathrm{L}}$ in terms of $\hat{\mathbf{R}}_i$:

$$\mathbf{U}_{\mathrm{R}} - \mathbf{U}_{\mathrm{L}} = \sum_{i=1}^{3} \hat{\alpha}_i \hat{\mathbf{R}}_i. \tag{60b}$$

Consequently, a $\mathcal{D}^{(p)}$ term is inserted, along with the $\mathcal{D}^{(\rho)}$ term, which can be easily seen from Eq. (50). It is exactly due to this process that the HLLEM inadvertently produces shock instability and violates the positively conservative condition, while the original HLLE scheme does not; see Obayashi and Wada [10].

We include in Fig. 7 the density contours, along with the profiles of variables (ρ, p, T) along the stagnation streamline of the supersonic blunt body problem. The AUSM$^+$ again yields clean and smooth solutions; the original AUSMDV has tiny nonmonotone contours near the stagnation streamline, which are now regularized after redefining the variable f in the mass flux. Although the carbuncle phenomenon produced by the Roe scheme is catastrophic, it can be completely cured with the modification, Eq. (57), that ensures $\mathcal{D}^{(p)} = 0\ \forall M$ in $\dot{m}$.

It was reported by Pandolfi and D'Ambrosio in [20] that elongation of cells in the direction normal to the shock would promote shock instabilities. The authors concluded that "methods that explicitly deal with the contact surface display a clear evidence of carbuncle phenomenon; if the interaction is very weak, or totally ignored, no carbuncle instability occurs." They further suggested that AUSM and AUSM$^+$ also suffered from the carbuncle phenomenon. Figure 8 shows the calculated results using both AUSM and AUSM$^+$ schemes for a Mach 20 flow on a 321×11 grid, which are twice as elongated as they used, 320×20. It is found that the shock position is stationary and remains smooth; the residual continues to drop toward machine zero. Notice that the result of the AUSM scheme displays a mild nonmonotonicity along the stagnation streamline, resulting in an indented contour, while the AUSM$^+$ result is monotonic (shown in Fig. 9). However, when using a second-order accurate procedure with limiters in the AUSM solution, the previous indented contour is cleared up and other contour lines become smoother.

Nevertheless, this nonmonotonicity must not be mistaken for the carbuncle phenomenon, or shock instabilities, because the latter will lead to a continued growth of disturbances, which is manifested by a continued expansion of the shock front, eventually reaching the outer boundary of the computation domain. Examples of these instabilities are displayed

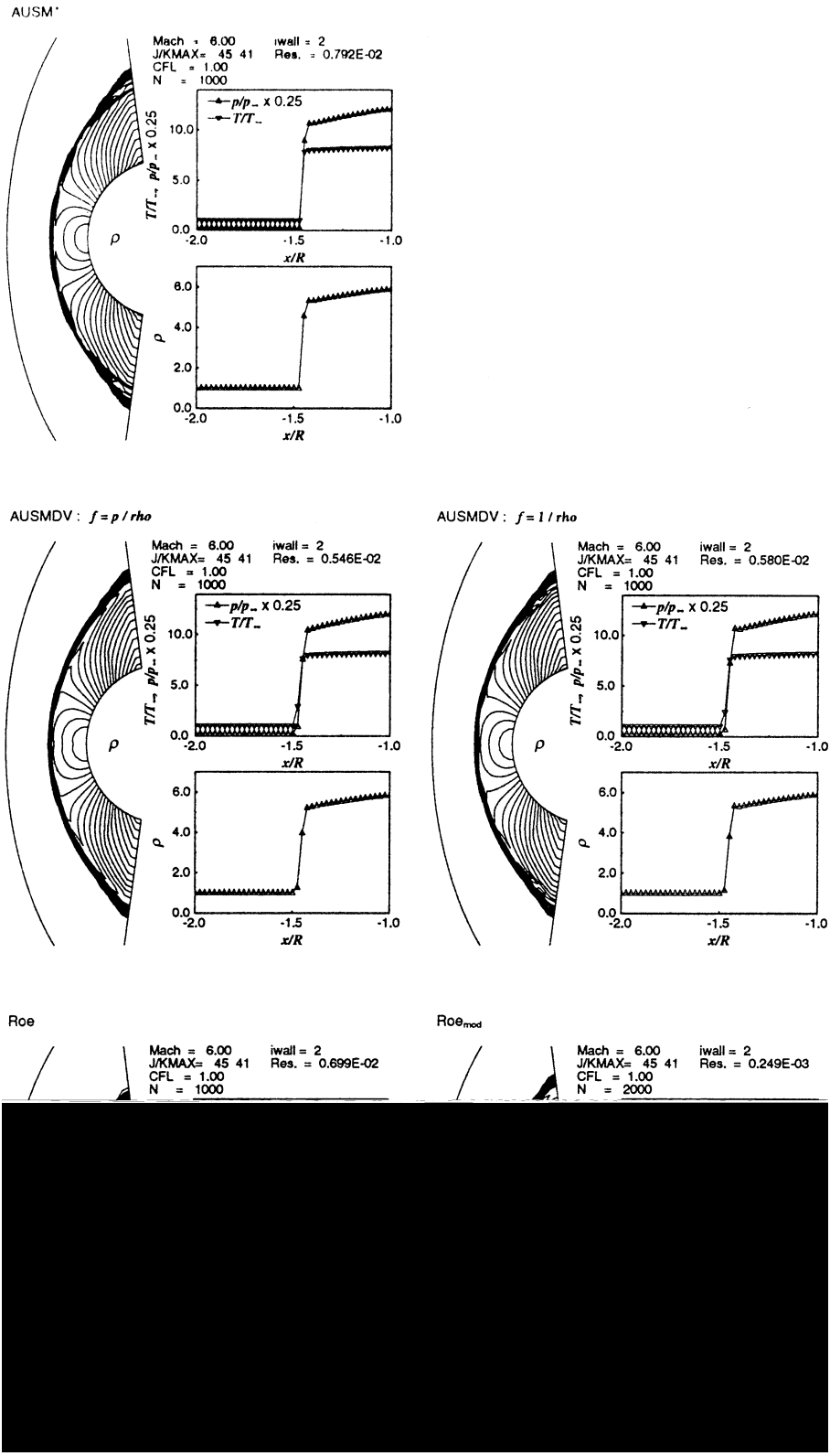

FIG. 7. Supersonic ($M_\infty = 6$) blunt body problem; profiles along the stagnation streamline.

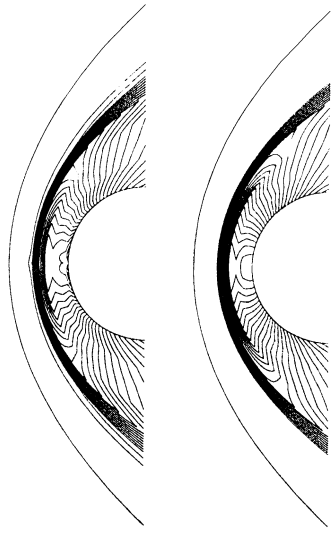

FIG. 8. Pressure contours of a Mach 20 flow over a cylinder on a 321×11 grid using the AUSM scheme. First-order (left) and second-order (right) accurate solutions.

in Figs. 7, 9, and 10 for the solution obtained by the Roe scheme. In Fig. 9, we display the enormously contaminated solution (left) after 2000 iterations and the resulting solution after continuing with the AUSM$^+$ scheme (middle), together with the convergence rate. From these results, we observe two interesting events: (1) once the initial phase of iterations is over, the convergence rate is identical, independent of the initial conditions, whether they be uniform or badly contaminated, and (2) the initial phase takes nearly the same number of iterations to smooth out the contamination as in the case of a uniform free stream condition. In this example, we see the interesting *self-correcting* property of the shock-stable scheme, AUSM$^+$.

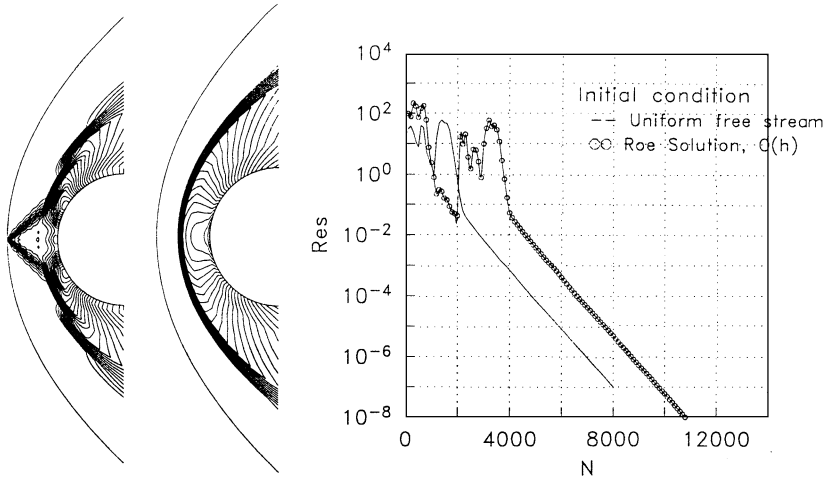

FIG. 9. Mach 20 flow over a cylinder on a 321×11 grid. Pressure contours obtained by the Roe scheme (left), the AUSM$^+$ solution (middle) obtained by continuing from the left carbuncle solution—showing the capability of correcting the contaminated solution. The residual histories of the AUSM$^+$ solutions from two different initial conditions are also included (right).

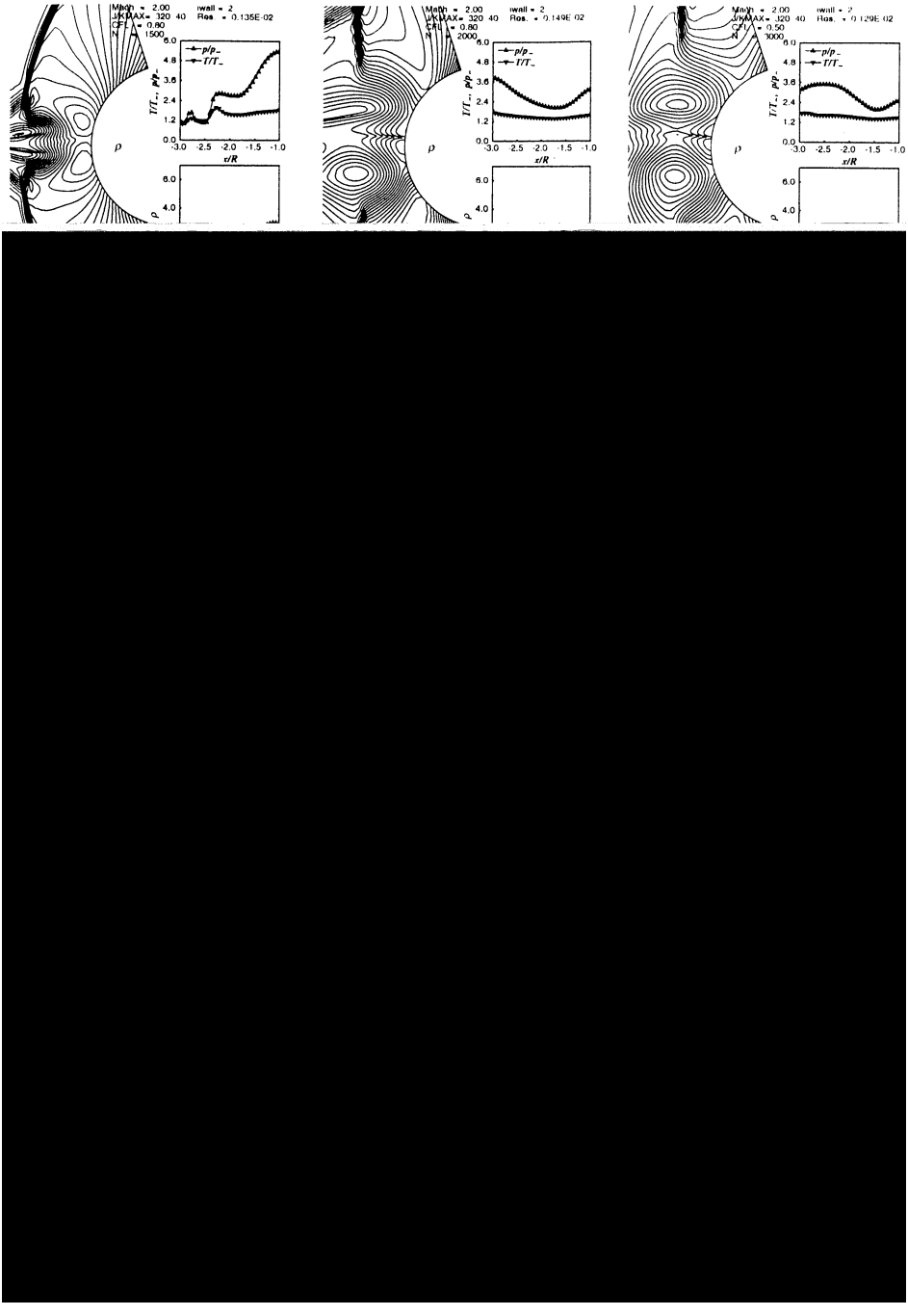

FIG. 10. Mach 2 flow over a cylinder on a 320×40 grid. Displayed are the formation of the carbuncle phenomena in the Roe solution (top row) and the correcting process by the AUSM$^+$ solution. Notice that the outward motion of the shock is reversed after the employment of AUSM$^+$ scheme. The shock has been pushed back to about one radius away from the cylinder after additional 1000 iterations. The remaining iterations reduce and smooth out disturbances, and finally approach a steady solution.

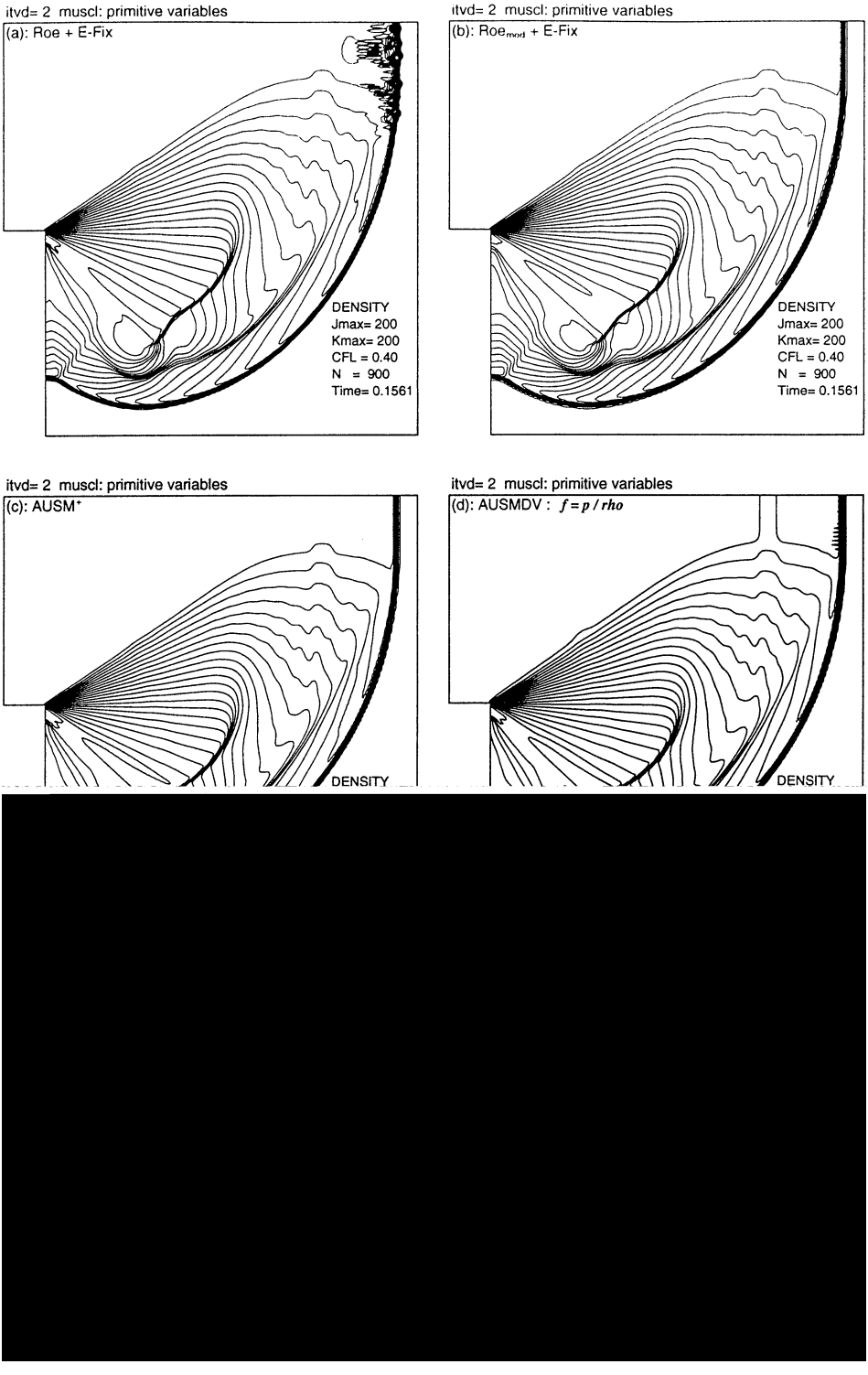

FIG. 11. Supersonic corner problem. The Roe flux with entropy fix produces shock instability which disappears after the modification enforcing $\mathcal{D}^{(p)} = 0$. A fine grid solution (at different instant) obtained with the AUSM$^+$ scheme is included for comparison, showing sharper resolution of shocks. All calculations were made with linear extrapolation of primitive variables using the Van Albada limiter.

This self-correcting property holds for low supersonic speeds as well. In Fig. 10, we display a detailed evolution of the solutions for a $M = 2$ flow on a 320×40 grid, at different iteration steps, initially obtained by the Roe scheme with the entropy fix and followed by the AUSM$^+$ scheme. It can be seen vividly how the Roe-flux solution deteriorated into a completely erratic situation and how this protuberant shock wave was pushed back toward the body and the disturbances were smoothed out, eventually reaching the correct steady-state solution. These and previous results suggest that the carbuncle phenomena occur throughout the supersonic range and the AUSM$^+$ scheme is capable of correcting them. This also suggests that the conjecture on the role of pressure term $\mathcal{D}^{(p)}$ may be valid for the entire range of $M > 1$.

Finally, we consider the diffraction of a shock moving supersonically over a 90° bend. In this calculation, a MUSCL-type linear interpolation of primitive variables is employed, along with the Van Albada limiter to maintain monotonicity. In contrast to the documented failings by several prominent flux schemes [9], the AUSM$^+$ flux demonstrates a robust shock-capturing capability, as displayed in Fig. 11. We note that although the entropy fix is sufficient for the Roe scheme to overcome the expansion fan at the corner, it is clearly useless in dealing with the shock-instability problem; see Fig. 11a. By the use of Eq. (57), the shock anomalies associated with the moving shock disappears, as seen in Fig. 11b. Included in Fig. 11 also is the AUSMDV solution (Fig. 11d); we can see at this instant a slight indication of irregularity along the straight stem of the primary shock, a situation similar to the Roe solution (Fig. 11a) but to a much lesser degree. The AUSM$^+$ solutions on two grids are shown in Figs. 11c and 11e to be robust and free of such shock instability; the fine grid solution defines discontinuities with more sharpness as expected.

Remark on the pressure diffusion term. There appears to be a strong belief that keeping the $\mathcal{D}^{(p)}$ term is beneficial, with which the author undoubtedly agrees. For example, it will eliminate pressure oscillations in the boundary layer or along the direction in which the velocity tends to zero, leaving very little numerical dissipation necessary to couple the velocity and pressure. The question to be posed, however, is whether or not it is *necessary* to have this term in the mass flux. My experience thus far has indicated that the $\mathcal{D}^{(p)}$ term is not necessary for moderate to high Mach numbers, but may be useful for very low Mach number flows. However, in the latter case, the shock instability question becomes an irrelevant point since there is not a shock to speak of.

5. CONCLUDING REMARKS

The mass flux, which is a factor common to all inviscid fluxes of conservation laws, is shown to be important in constructing a numerical flux. A detailed analysis of the numerical mass flux has proven to be very enlightening, and especially helpful for the purpose of designing a shock-stable scheme.

A number of mass flux schemes have been examined, especially with regard to the role of the dissipative pressure term. It is confirmed that this term is the root for causing the carbuncle and the odd–even decoupling phenomena that we classify as shock instabilities. These types of shock instabilities are multidimensional in nature because in one space dimension, the shock front is planar and no irregularities are allowed to occur in the second/third directions.

As a consequence of the proposed Conjecture, we have suggested a fix to free the Roe scheme from developing these instabilities. Furthermore, we demonstrated the self-correcting capability of a shock-stable scheme with respect to the carbuncle-contaminated profiles. We also have shown that the carbuncle phenomena occur not only in the high Machr-number flows, but also in the low supersonic Mach numbers.

APPENDIX

COROLLARY. *In the HLLE scheme,*

$$u_L - b^- \geq a_L \qquad \textit{and} \qquad u_R - b^+ \leq -a_R. \tag{A.1}$$

Proof. Since $b^- = \min(0, b_L)$, we have

$$u_L - b^- = \begin{cases} u_L, & \text{if } b_L \geq 0, \\ u_L - b_L, & \text{otherwise.} \end{cases} \tag{A.2}$$

From $b_L = \min(\hat{u} - \hat{a}, u_L - a_L)$, we can further show:

1. $b_L \geq 0$; thus $u_L \geq a_L$, since every argument in b_L must be nonnegative.
2. $b_L < 0$; then

$$u_L - b_L \begin{cases} = a_L, & \text{if } u_L - a_L \leq \hat{u} - \hat{a}, \\ > a_L, & \text{otherwise.} \end{cases} \tag{A.3}$$

Hence,

$$u_L - b^- \geq a_L \geq 0. \tag{A.4}$$

Similarly, one can readily show

$$u_R - b^+ \leq -a_R \leq 0. \tag{A.5}$$

This completes the proof.

ACKNOWLEDGMENTS

The author is grateful to the reviewers for their comments which have led to improvements of the paper. The support given by the Computing and the Interdisciplinary Systems Office, NASA Glenn (formerly Lewis) Research Center is acknowledged.

REFERENCES

1. S. K. Godunov, A difference method for the numerical calculation of discontinuous solutions of hydrodynamic equations, *Mat. Sb.* **47**, 271 (1959) (translation, US JPRS: 7225, November 1960).
2. Y. Wada and M.-S. Liou, An accurate and robust flux splitting scheme for shock and contact discontinuities, *SIAM J. Sci. Comput.* **18**, 633 (1997).
3. M.-S. Liou, Probing numerical fluxes: Mass flux, positivity, and entropy-satisfying property, AIAA paper 97-2035-CP (1997).

4. P. L. Roe, Approximate Riemann solvers, parameter vectors, and difference schemes, *J. Comput. Phys.* **43**, 357 (1981).
5. S. Osher and F. Solomon, Upwind difference schemes for hyperbolic systems of conservation laws, *Math. Comp.* **38**, 339 (1982).
6. B. van Leer, Flux-vector splitting for the Euler equations, in Lecture Notes in Physics, Vol. 170 (Springer-Verlag, Berlin, 1982), p. 507.
7. D. Hänel, R. Schwane, and G. Seider, On the accuracy of upwind schemes for the solution of the Navier–Stokes equations, AIAA paper 87-1105-CP (1987).
8. B. Einfeldt, On Godunov-type methods for gas-dynamics, *SIAM J. Numer. Anal.* **25**, 294 (1988).
9. B. Einfeldt, C. D. Munz, P. L. Roe, and B. Sjögreen, On Godunov-type methods near low densities, *J. Comput. Phys.* **92**, 273 (1991).
10. S. Obayashi and Y. Wada, Practical formulation of a positively conservative scheme, *AIAA J.* **32**, 1093 (1994).
11. M.-S. Liou, A sequel to AUSM: AUSM$^+$, *J. Comput. Phys.* **129**, 364 (1996).
12. M.-S. Liou and C. J. Steffen, A new flux splitting scheme, *J. Comput. Phys.* **107**, 23 (1993).
13. J. J. Quirk, A contribution to the great Riemann solver debate, *Internat. J. Numer. Methods Fluids* **18**, 555 (1994).
14. F. Coquel and M.-S. Liou, Hybrid upwind splitting (HUS) by a field-by-field decomposition, NASA TM 106843 (1995).
15. E. Shima and T. Jounouchi, AUSM type upwind schemes, preprint, 1996.
16. R. C. Swanson, R. Radespiel, and E. Turkel, On some numerical dissipation schemes, *J. Comput. Phys.* **147**, 518 (1998).
17. K. M. Peery and S. T. Imlay, Blunt-body flow simulations, in *AIAA/SAE/ASME/ASEE 24th Joint Propulsion Conference, 1988*; AIAA paper 88-2904.
18. H.-C. Lin, Dissipation additions to flux-difference splitting, in *10th AIAA Computational Fluid Dynamics Conference, 1991*; AIAA paper 91-1544.
19. J. R. Edwards, A low-diffusion flux-splitting scheme for Navier–Stokes calculations, *Comput. & Fluids* **26**, 635 (1997).
20. M. Pandolfi and D. D'Ambrosio, Upwind methods and carbuncle phenomenon, in *Proceedings of the Fourth European Computational Fluid Dynamics Conference* (Wiley, New York, 1998), p. 126.
21. A. Jameson, Analysis and design of numerical schemes for gas dynamics. II. Artificial diffusion and discrete shock structure, *Internat. J. Comput. Fluid Dynamics* **5**, 1 (1995).
22. R. Sanders, E. Morano, and M. Druguet, Multidimensional dissipation for upwind schemes: Stability and applications to gas dynamics, *J. Comput. Phys.* **145**, 511 (1998).